Available online at www.sciencedirect.com

ScienceDirect

Journal of the European Ceramic Society 29 (2009) 2297–2308

www.elsevier.com/locate/jeurceramsoc

# Quantitative microstructural analysis and piezoelectricity of highly dense, submicron-structured $NaNbO_3$ ceramics from mechanically activated precursors

A. Moure[a,*], T. Hungría[b], A. Castro[b], L. Pardo[b]

[a] Instituto de Cerámica y Vidrio, CSIC, C/Kelsen, 5, 28049 Madrid, Spain
[b] Instituto de Ciencia de Materiales de Madrid, CSIC, Cantoblanco, 28049 Madrid, Spain

Received 20 October 2008; received in revised form 14 January 2009; accepted 15 January 2009
Available online 23 February 2009

## Abstract

We study in this work the processing of $NaNbO_3$ ceramics prepared in a single thermal treatment of highly reactive precursors obtained by mechanical activation of different reagents, aiming to determine optimum conditions for piezoelectric ceramics production. Pressure-less sintering at 1200 °C leads to dense ceramics (<5% porosity) with poor mechanical stability, unsuitable for practical uses. Dense hot-pressed ceramics were also obtained at lower temperatures (900–1100 °C), all of them in the submicron range of average grain sizes (<400 nm). Their microstructure was quantitatively characterized and their elastic and electromechanical properties determined by an automatic iterative method from impedance measurements at resonance. A noticeable ensemble of piezoelectric and elastic properties ($d_{33} = 38\,pC\,N^{-1}$ and $N_p = 3252\,kHz\,mm$) was measured for hot-pressed ceramics, from precursors obtained by a combined route of wet-chemistry and mechanical activation, with a microstructure characterized by 0.4% residual porosity and a bimodal lognormal distribution of grain size.

*Keywords:* Quantitative microstructure analysis; Mechanical activation; Piezoelectricity; Niobates

## 1. Introduction

There is a recent need[1] for finding environmentally friendly lead-free piezoceramics with properties comparable with the ones of the commercial piezoceramics, based mainly in lead compounds. In this sense, alkaline niobates have been considered good candidates as an alternative for this substitution.[2–4] However, the processing of ceramics with alkaline-niobate compositions by classical methods has traditionally shown difficulties in obtaining densities near the theoretical.[5,6] The classical method for obtaining alkali metal niobate powders by a solid-state reaction between $Nb_2O_5$ and alkali metal carbonates involves high temperatures and long reaction times that produces the volatilisation of the alkaline metal, leads to poor compositional homogeneity and provides precursors with large particles. Traditionally, hot-pressing at high temperatures[7] and more recently other pressure- or electric field-assisted methods as the spark plasma sintering[8,9] of precursors obtained by solid-state reaction or other alternative methods are needed to increase the density of the ceramics.

Sodium niobate ($NaNbO_3$), within the series of alkaline-niobate compounds, is antiferroelectric at room temperature.[10] The application of an electric field, or the substitution of Na by Li[5] or K,[11] induce a ferroelectric phase that provides piezoelectric activity, of interest mainly for high frequency devices. Beside the improvement in piezoelectric activity, solid solutions with Li- or K-based niobate are often required to improve the processing of the ceramics with respect to the $NaNbO_3$ pure ones.[7] Thus, an important goal in the study of alkaline-niobate ceramics is to solve the difficulties in the $NaNbO_3$ processing, as a way to enhance its piezoelectricity, as well as to allow a further improvement of properties in the $NaNbO_3$-based solid solution ceramics through the control of its microstructure.

Due to the problems in the processing of these ceramics by traditional methods, alternative routes have to be developed to facilitate the production of desired alkaline-niobate ceramics in a controllable way. Powder synthesis using evaporation,[12] sol–gel,[13] hydrothermal (both simple[14]

---

* Corresponding author. Fax: +34 91 735 5843.
*E-mail address:* alberto.moure@icv.csic.es (A. Moure).

0955-2219/$ – see front matter © 2009 Elsevier Ltd. All rights reserved.
doi:10.1016/j.jeurceramsoc.2009.01.016

or microwave-assisted[15]), polymeric precursor processes,[16] microemulsion mediated hydrolytic decomposition of mixed alkoxide solutions[17] or coprecipitation[18] have been described in the literature to facilitate the reactions. Densities even near the theoretical one have been achieved by some of these methods,[12] although piezoelectric characterization of pure $NaNbO_3$ is not reported in these works. These chemistry based routes require high purity inorganic or organometallic reactants, that are often sensitive to light or humidity and are more expensive than the widely available oxides and carbonates.

Mechanochemical activation has shown to be a successful way to modify the conditions in which chemical reactions usually take place. It has been applied to produce the synthesis of known functional lead-based (PZT,[19] PMN-PZT-PT,[20] PZN-PT[21]) and other lead-free[22,23] piezoceramics, with $Bi_4Ti_3O_{12}$ composition. A thorough review of the application of this route to ferroelectric materials in general has been recently published.[24] During the mechanical treatment the particle size of the crystals is reduced and the homogeneity of the mixture is increased. It improves the reactivity of the precursors[25] and allows the compact of the green pellet to be optimised. The processing of highly dense ceramics,[26–28] is possible in a single thermal process, in which synthesis, grain growth and sintering take place.

Mechanochemical activation has been proved to be an adequate route to synthesis $NaNbO_3$ compositions. Recently, it was shown[29] that mechanosynthesis takes place by milling after 40 h of a powder mixture of $Na_2CO_3$ and $Nb_2O_5$, although the final mixture contains large amounts of amorphous phases and residual traces of the initial mixtures. The same authors have also studied the effect of different milling energies[30] on the same mixtures. X-ray diffraction (XRD) shows peaks only corresponding to $NaNbO_3$ composition after 400 h of milling, for vials and balls of yttria-stabilized zirconia (YSZ). Time needed for isolate $NaNbO_3$ can be reduced to 96 h by using tungsten carbide vials with heavier balls rotated at higher speed (5 rps against 3.3 rps for YSZ media). However, the influence of the mechanical activation on the sintering, microstructure and piezoelectric properties of the ceramics has not yet been determined. This is an important feature because, as will be shown in this work, it is needed, but not sufficient, to have reactive precursors to obtain good piezoelectric ceramics and ways for the ceramic microstructure control are also required.

It is known that the piezoelectricity in ferroelectric ceramics depends on their microstructure (porosity, grain and domain size).[31–33] The expected reduction of the processing temperature of the ceramics from precursors obtained by mechanical activation should result in a microstructure with reduced grain size, while the pressure applied and high reactivity and specific surface of the nano-sized particles of the powder should maintain porosity values within the limits required for piezoelectric applications. Although in the last years there has been an increasing interest in the topic, the size effects in the functional properties of these alkaline-niobate materials are barely found in the literature. Connected to this topic, some interesting features have been recently reported. It was shown that the reduction of the $NaNbO_3$ particles to submicron size (200–400 nm) induces a non-centrosymmetric phase that improves the piezoelectric properties, as PFM studies of displacement against voltage shows.[34,35]

In this work, a quantitative study of the microstructure of highly dense submicron-structured $NaNbO_3$ ceramics, obtained from four different mechanically activated precursors has been carried out. An iterative method was applied to determine the complex piezoelectric, elastic and dielectric coefficients of the ceramics from complex impedance measurements at the planar resonance of thin ceramic disks. The relation between processing, microstructure and piezoelectric and elastic properties is discussed.

## 2. Experimental procedure

$NaNbO_3$ ceramics have been prepared from precursors obtained by four different routes. The rationale behind the compositions selected and the details of the precursor processing and characterization can be found elsewhere.[36] Summarizing, stoichiometric mixtures of analytical-grade $Nb_2O_5$ and sodium reactants ($Na_2CO_3$, $Na_2O$ or NaOH) were mixed by hand in an agate mortar. The mixture of $Nb_2O_5$–$Na_2CO_3$ (hereinafter C-NN) was mechanically activated during 30 days, whereas to obtain similar degree[36] of XRD amorphization, the mixtures $Nb_2O_5$–$Na_2O$ (hereinafter O-NN) and $Nb_2O_5$–NaOH (hereinafter NOH-NN) were activated for only 7 days. For the fourth precursor, a mixed technique of wet-chemistry plus mechanochemical activation was used. NaOH was dissolved in deionised water and the stoichiometric quantity of $Nb_2O_5$ was added into the aqueous solution. This suspension was stirred for 4 h and then dried at 150 °C overnight, to obtain the precursor for the mechanical activation process, hereinafter called DOH-NN.

Ceramics were obtained by a single thermal treatment under different conditions. Precursors powders were shaped by uniaxial pressing at 210 kg $cm^{-2}$ as thin disks of 10 mm diameter and 2 mm thickness, approximately. Disks were isostatically pressed at 2000 kg $cm^{-2}$ and then pressure-less sintering was carried out on a Pt foil at 1200 °C for 2 h. Alternatively, disks were uniaxially hot-pressed at ~200 kg $cm^{-2}$ in alumina dies and surrounded by alumina powder at temperatures of 900, 1000 °C and 1100 °C. Hot-pressing time was 2 h in all cases, except for the ceramic processed at 900 °C from C-NN precursors (1 h).

XRD patterns at room temperature were measured in a D500 Siemens Diffractometer, between $2\theta = 20$–$50°$, with a step of 0.05° and counting time of 0.5 s/step.

Quantitative microscopy characterization was carried out with a computerised image analysis and measurement system (IMCO10-KAT386 system, Kontron Elektronic GMBH, 1990) by a procedure explained in detail elsewhere.[37] Ceramic surfaces were polished and analysed by optical microscopy (Leitz Laborlux 12 ME S/ST), in order to examine the ceramic porosity. The percentage of porosity was characterized by the fraction of the examined area which is occupied by pores. The pore size ($P$) was characterized by the pore area, since the shape greatly varies from sample to sample. The experimental error of these measurements is $\pm 0.1\ \mu m^2$. The average and standard deviation of the distributions of pore size were obtained from the linear fitting of the experimental data represented in probability plots.[38] In these plots, the Ln of the variable being studied is represented against the corresponding cumulative frequency in a probability scale. Linear fitting of the obtained plot provides the size distribution characteristics and demonstrates the single or bimodal character of the distribution.[37]

Polished ceramic surfaces were etched from 800 or 900 °C to room temperature for the study of the grain distribution. Due to the submicron range of grain size of all ceramics, scanning electron microscopy (960 Zeiss SEM apparatus) was necessary to obtain surface images of the etched ceramics. The ceramic grain size ($G$) was characterized by the equivalent diameter to a circular shape, a valid approximation for all samples, and calculated from the measured grain area as: $D_{\mathrm{eq}} = (4\ \mathrm{Area}/\pi)^{1/2}$. The experimental error of these measurements is ±20 nm. The average and standard deviation of the distributions of equivalent diameter were also obtained from the corresponding probability plots.

Electroded ceramic samples of diameter ($D$) ~10 mm were grounded to a 0.7–1.0 mm thickness ($t$) to obtain a sample with a $D/t$ ratio ~10. Pt paste was sintered at 700 °C in the major sample surface electrodes, and then ceramics were poled to saturation in a silicon oil bath at 120–180 °C, with fields up to 60 kV/cm. The piezoelectric $d_{33}$ coefficient was measured in a Berlincourt-meter by the direct piezoelectric effect at 100 Hz. Dielectric ($\varepsilon'_{33}$), elastic ($s^{E}_{11}$) and piezoelectric complex coefficients ($d_{31}$), as well as electromechanical coupling factors ($k_p$) corresponding to the radial vibration mode of the disks were measured by an automatic iterative method described elsewhere,[39] from complex impedance measurements at resonance using a HP4192A impedance analyser.

## 3. Results

Fig. 1 shows the X-ray diffraction patterns of ceramics pressure-less sintered at 1200 °C from C-NN, O-NN and DOH-NN precursors. The intensity axis is represented after normalization to 1, so comparison can be directly done. In all cases, a single $NaNbO_3$ (JCPDS-ICDD file no. 33-1270) phase is obtained, indicating that it is possible to have ceramics in a single sintering thermal treatment, and that no decomposition occurs at that temperature.

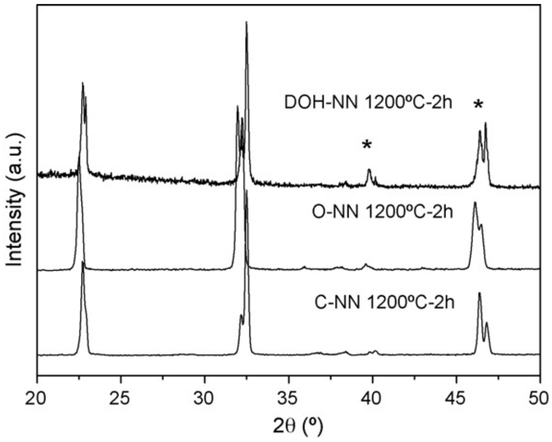

Fig. 1. XRD patterns of pressure-less sintered $NaNbO_3$ ceramics from mechanically activated precursors. [Peak marked with (*) corresponds to Pt, remaining from electrode.]

Fig. 2a and b show the polished surfaces of ceramics sintered at 1200 °C from O-NN and DOH-NN precursors, respectively. In the case of C-NN precursors, it is also possible to get single-phase ceramics, as Fig. 1 shows. However, the density obtained by measurements of dimensions and mass is as low as 45% of the theoretical one, even lower than the green pellet density (63%). It makes impossible to polish the surfaces, and quantitative microstructure analysis has not been carried out in those types of ceramics.

While polishing, it was observed that the mechanical stability of the DOH-NN and the O-NN ceramics was very poor. Pull-out and cracking occurred even at the smoothest steps of polish (0.1 μm $Al_2O_3$ emulsion). It makes impossible the use of these sintered ceramics in any further piezoelectric applications. To improve the mechanical stability, and with the aim to preserve a single thermal step process, hot-pressing was applied to obtain mechanically stable and dense ceramics.

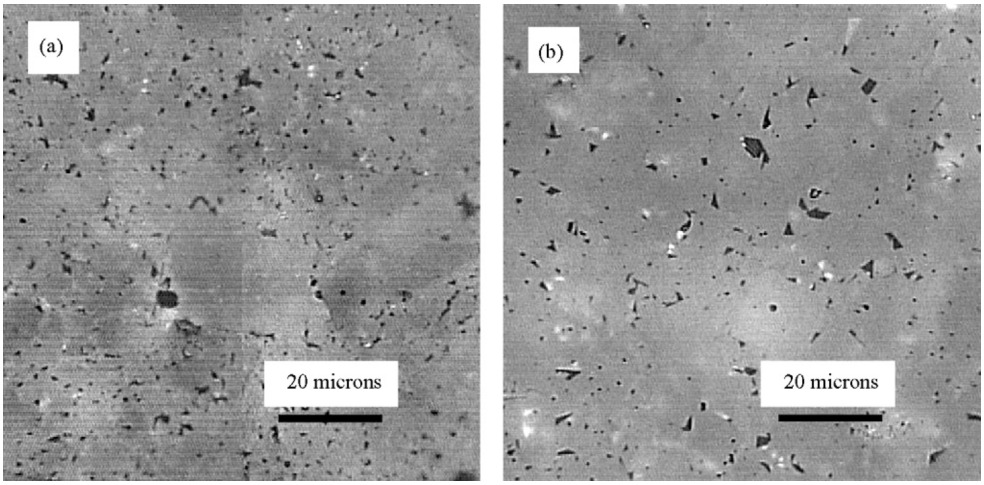

Fig. 2. Optical micrographs of the polished surfaces of $NaNbO_3$ ceramics pressure-less sintered at 1200 °C from (a) O-NN and (b) DOH-NN precursors.

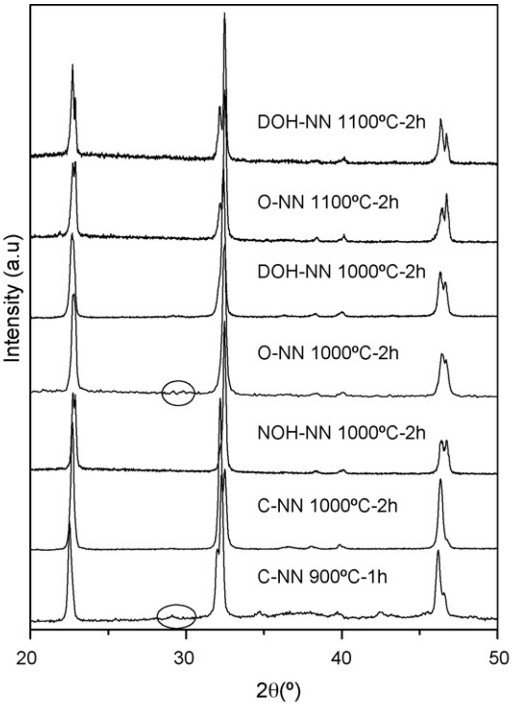

Fig. 3. XRD patterns of hot-pressed $NaNbO_3$ ceramics from mechanically activated precursors. [Peak marked with a circle corresponds to a $Na_2Nb_4O_{11}$ phase.]

Fig. 3 shows the X-ray diffraction patterns of ceramics hot-pressed at 900 °C (1 h) from C-NN, 1000 °C from C-NN, O-NN, NOH-NN and DOH-NN, and 1100 °C for O-NN and DOH-NN precursors. As for Fig. 1, the intensity is represented after normalization to 1. All of them are single-phase ceramics, except the C-NN and O-NN hot-pressed at 900 and 1000 °C, respectively. A peak corresponding to a trace of a secondary phase is marked with a circle.

Fig. 4 shows the polished surfaces of the hot-pressed ceramics. All of them present close porosity, except the hot-pressed at 1000 °C from O-NN. This ceramic presents two types of pores, one coming from room among the agglomerates (open porosity) and the other from inside them. The increase in the processing temperature in C-NN to 1000 °C and O-NN to 1100 °C decrease the porosity. There is an opposite trend for the DOH-NN, in which an increase of hot-pressing temperature from 1000 to 1100 °C increases both the porosity and the number of pores, as corresponds to a beginning of a degraded sintering stage.[37]

Fig. 5a shows the probability plots of the pore area of the ceramics shown in Fig. 1. The slope of the line for the DOH-NN ceramic is shifted to lower values, meaning wider pore area distribution. From the micrographs and the probability plots, values of content of porosity, mean value and standard deviation of the pore size distributions are calculated. The results are shown in Table 1. Porosity is slightly lower for the DOH-NN ceramic (3.0%) than for the O-NN one (4.5%), but it has larger mean pore size values.

As for the pressure-less sintered ceramics, the Fig. 5b shows the probability plot of the pore area of hot-pressed ceramics. The slope of the ceramics hot-pressed at 900 °C from C-NN, and 1000 °C from O-NN are lower, and the cut with the *x*-axis decreases. The slopes are very similar for the rest of the ceramics. Table 1 also shows the values of content of porosity, and the mean value and standard deviation of the pore size distributions obtained from the probability plots of Fig. 5b. The porosity is higher for the C-NN and O-NN precursors, and it is lower for the DOH-NN one. In this case, values of porosity as low as 0.40% and 2.10% are obtained by hot-pressing at 1000 and 1100 °C, respectively.

The measurement of the porosity of ceramics from polished surfaces is a technique successfully used in previous works.[37,40–42] For both the pressure-less sintered and the hot-pressed ceramics studied in this work, the linear fit of the probabilistic plot of the pore area proves that the objects measured are really pores, and not artificial elements. The content of porosity shown in Table 1, measured from the micrographs, can thus be taken as good, within experimental error.

The problems during polishing for pressure-less sintered ceramics do not appear in hot-pressed ceramics. The polished ceramics were then etched in order to study the grain size. The ceramic hot-pressed at 900 °C from C-NN precursors was not

Table 1

Pore size distribution parameters of pressure-less sintered and hot-pressed $NaNbO_3$ ceramics. The error quoted is the highest among the experimental and calculation values.

| Pore distribution | | | | | |
|---|---|---|---|---|---|
| Precursor | Sintering temperature | Mean pore size $P$ ($\mu m^2$) | Standard deviation $\sigma_P$ ($\mu m^2$) | Porosity (%) | Number of measured pores $N_p$ |
| Pressure-less sintered ceramics | | | | | |
| O-NN | 1200 °C | 0.7 ± 0.1 | 0.5 ± 0.1 | 4.5 ± 0.2 | 762 |
| DOH-NN | 1200 °C | 1.3 ± 0.1 | 1.6 ± 0.1 | 3.0 ± 0.3 | 1230 |
| Hot-pressed ceramics | | | | | |
| C-NN | 900 °C (1 h) | 10 ± 2 | 18 ± 2 | 33.7 ± 0.5 | 800 |
| | 1000 °C | 0.7 ± 0.1 | 0.7 ± 0.1 | 6.4 ± 0.8 | 1572 |
| NOH-NN | 1000 °C | 0.6 ± 0.1 | 0.4 ± 0.1 | 1.5 ± 0.1 | 616 |
| O-NN | 1000 °C | 4.2 ± 0.8 | 47 ± 17 | 6 ± 4 | 526 |
| | 1100 °C | 0.9 ± 0.1 | 0.7 ± 0.1 | 3.8 ± 0.3 | 1790 |
| DOH-NN | 1000 °C | 0.6 ± 0.1 | 0.6 ± 0.1 | 0.40 ± 0.02 | 376 |
| | 1100 °C | 0.4 ± 0.1 | 0.2 ± 0.1 | 2.10 ± 0.06 | 1274 |

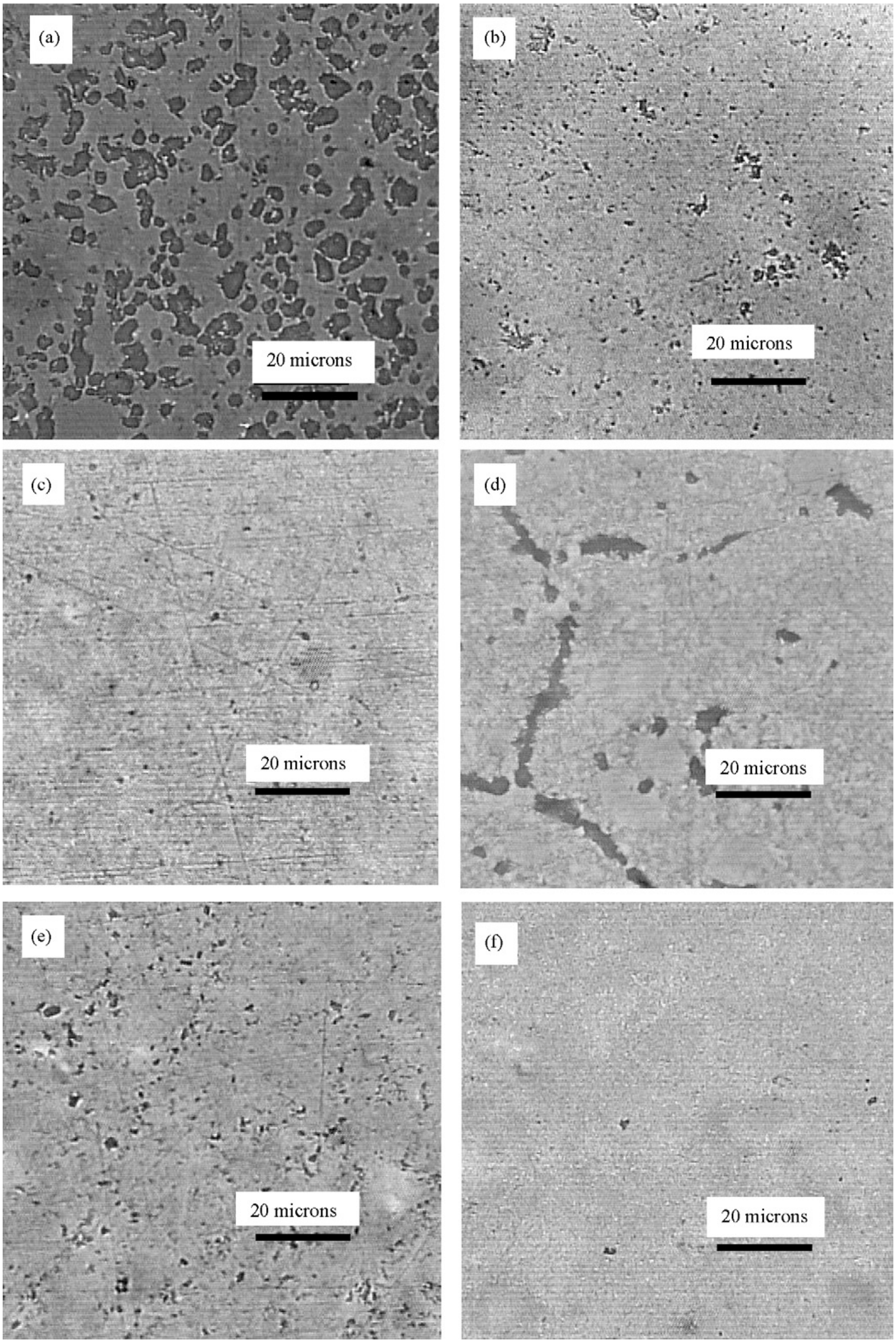

Fig. 4. Optical micrographs of the polished surfaces of hot-pressed $NaNbO_3$ ceramics from mechanically activated precursors: (a) C-NN, 900 °C (1 h); (b) C-NN 1000 °C; (c) NOH-NN 1000 °C; (d) O-NN 1000 °C; (e) O-NN 1100 °C; (f) DOH-NN 1000 °C; (g) DOH-NN 1100 °C.

measured, because its high porosity (33.7%) reduces its practical interest, in comparison with the other ceramics studied. Fig. 6 shows the aspect of the etched surfaces of the rest of hot-pressed ceramics. The ceramics processed at 1000 °C from O-NN and from DOH-NN, are inhomogeneous, but the nature of this inhomogeneity is slightly different. In the O-NN case, a clear bimodal distribution with two families of grains that seems to be entirely formed is observed, showing remarkable difference in grain size of the two families. The surface percentage of occupancy of the higher grain size family is 35%, approximately. Ultra-fine intergranular porosity accompanies the family of smaller grain sizes. This ultra-fine porosity, which was not observed at the magnifi-

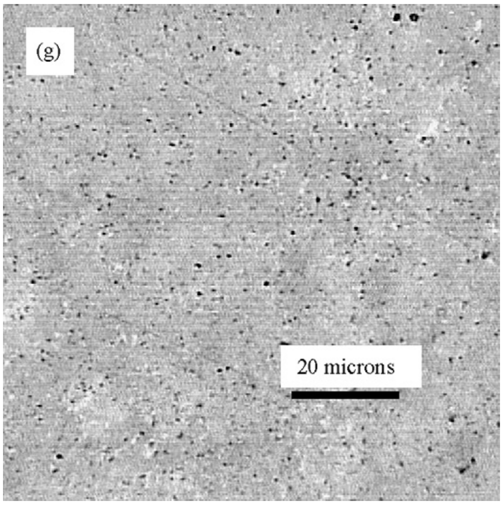

Fig. 4. (*Continued*).

cation of Fig. 4d, was not taken into account for the measurement of pore size distribution. Such ultra-fine porosity, which is also negligible when calculating the total percentage of porosity is, however, detrimental for the grain connectivity needed for the establishing of a homogeneous electric field in the ceramic.

The DOH-NN ceramic hot-pressed at 1000 °C presents a more complex microstructure comprising three families of objects with characteristic sizes. One of them consists of well formed grains, similar to the grains of the more homogeneous microstructures in Fig. 6. Those grains are marked with an asterisk in Fig. 6 for DOH-NN 1000 °C ceramic. They occupy approximately 50% of the area of the ceramic surface analysed. Another family of objects consists of clusters, with an internal structure, from which the well formed grains most probably grow as the sintering progresses. Finally, the third family of objects will be the very fine grains in coalescence that constitute the internal structure of the clusters. These are well connected and do not show intergranular porosity. This ceramic presents also an overall fully dense aspect (Fig. 4f).

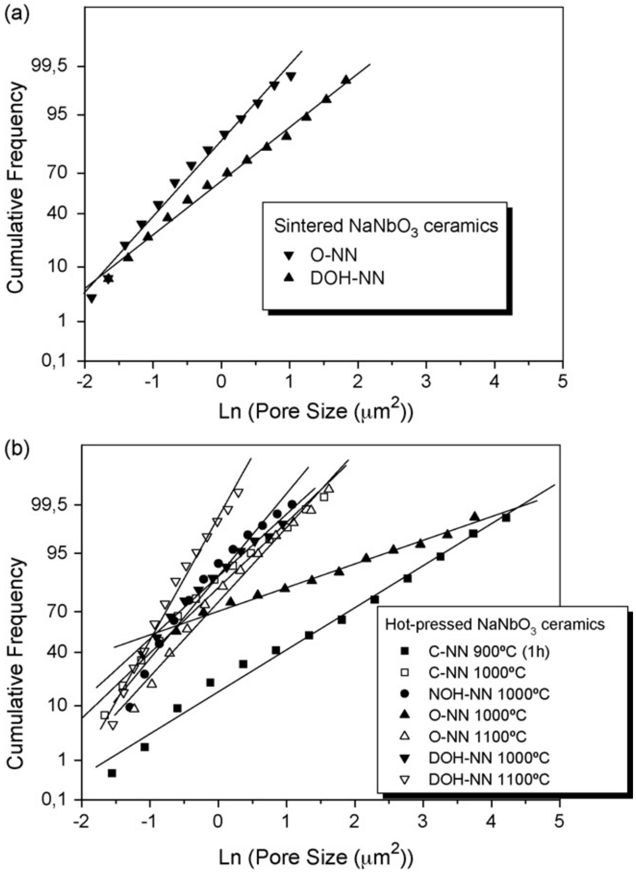

Fig. 5. Probably plots of pore size for surfaces of pressure-less sintered and hot-pressed NaNbO$_3$ ceramics.

The increase of the hot-pressing temperature to 1100 °C increases the homogeneity in grain distribution for both O-NN and DOH-NN ceramics (Fig. 6).

Figs. 7 and 8 shows the probability plots of the grain size distributions of hot-pressed ceramics. Fig. 7 also shows the original distributions of grain size for the two ceramics with complex microstructures discussed above: the ceramics obtained at 1000 °C from O-NN and from DOH-NN. The good linear fit of the cumulative frequency vs. natural logarithm of the grain size proves the accuracy of the measurement. The measured objects are grains representative of the bulk, and not other artificial objects, appearing for example during thermal etching.

A strong change in the slope of the probability plot is observed for the O-NN 1000 °C ceramic, showing the bimodal character of the distribution of the logarithm of grain size. The linear fitting showed provides the average and standard deviation of the population of smaller grain size, which are shown in Table 2. There is not a statistical sample of the population of larger grains at the magnification of Fig. 6, and the quantitative analysis was not carried out for this population.

For the also complex microstructure of DOH-NN 1000 °C ceramic, only the distribution that correspond to the population of grains marked with asterisk in Fig. 6 is showed and quantitatively characterized in Fig. 7 and Table 2. The method here used lacks experimental resolution for the measurement and analysis of the population of smaller grains in coalescence. However, their average grain size must be much lower than the one for the population of small grain sizes for the O-NN 1000 °C ceramic, as can be clearly observed by comparison of the corresponding micrographs in Fig. 6, i.e., must be well below 100 nm.

The analysis by probability plots of all the other grain size single distributions of hot-pressed ceramics are shown in Fig. 8 and Table 2. The linear relation between the cumulative frequency and the logarithm indicates again that all of them are lognormal distributions. The slopes move to higher values as the hot-pressing temperature increases, 1000 °C in Fig. 7 and 1100 °C in Fig. 8, due to the observation of narrower distributions, corresponding to more homogeneous microstructures. For the sake of comparison with the distributions of the complex microstructures in Figs. 7 and 8 shows the grain size distribution of the most homogeneous ceramic microstructure obtained, for DOH-NN 1100 °C.

Table 2 also shows the piezoelectric $d_{33}$ coefficients, which depend on the microstructure of the ceramics. The ceramics

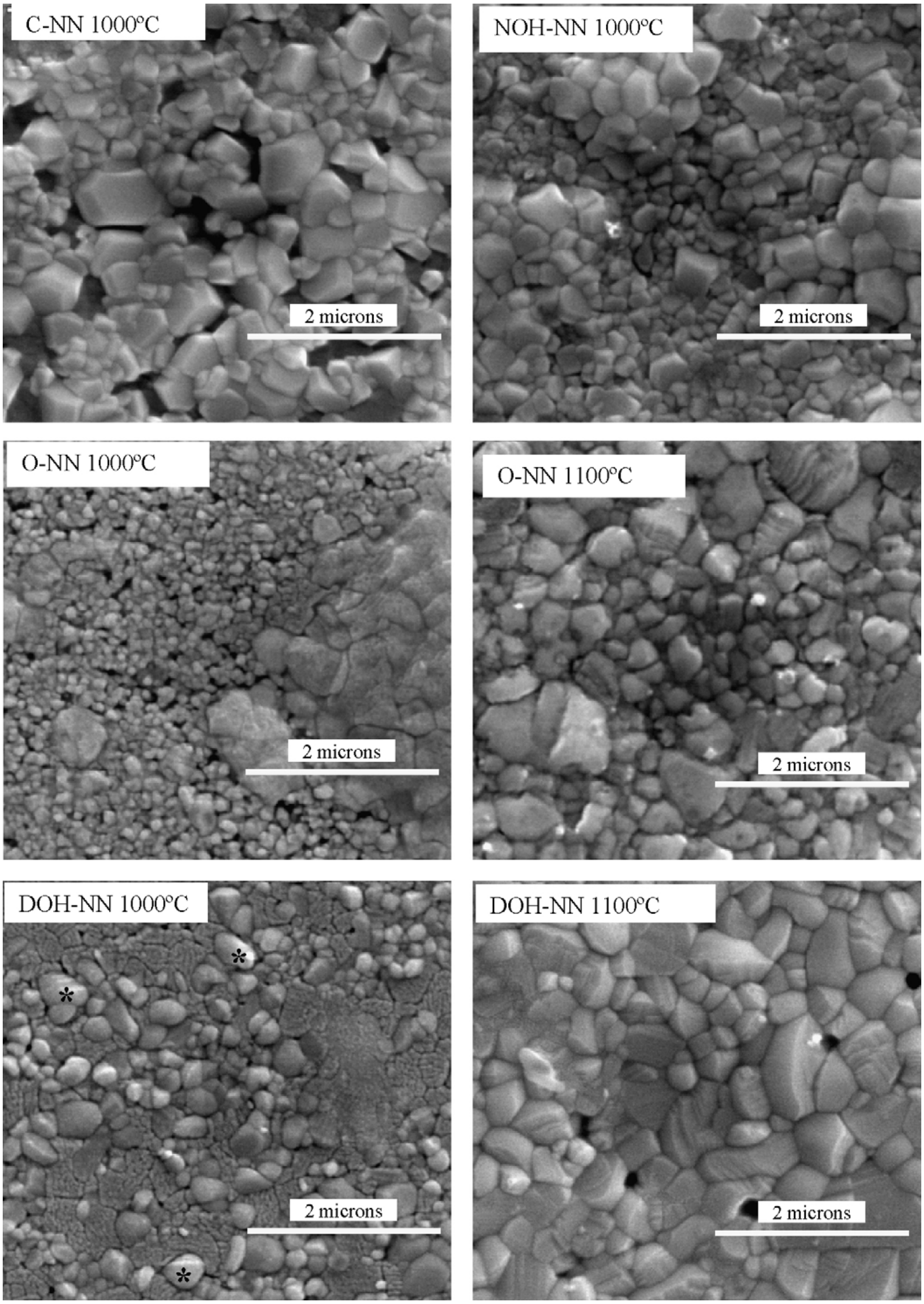

Fig. 6. SEM micrographs of polished and thermally etched surfaces of hot-pressed $NaNbO_3$ ceramics.

hot-pressed at 1000 °C from O-NN and NOH-NN, which show a combination of a very low average size for the population of small grains (110 nm) and insufficient grain connectivity for the former, and the lowest average value for a single grain size distribution (170 nm) for the latter, are difficult to pole. Their $d_{33}$ coefficients are the lowest ($6\,pC\,N^{-1}$) of all the measured ceramics.

Table 3 shows the complex dielectric, elastic, piezoelectric and electromechanical coupling factors corresponding to the radial resonance mode of poled ceramic disks at room temperature. Only the ceramics with the highest values of $d_{33}$ (Table 2) were chosen to be studied. It is noticeable that properties of all ceramics are similar and only small differences among them are observed. The ceramic from C-NN (hot-pressed at 1000 °C) has the highest piezoelectric coefficient ($d_{31} = -8.7\,pC\,N^{-1}$) and electromechanical activity ($k_p = 14\%$). The ceramic hot-pressed at 1100 °C from DOH-NN precursor presents the highest elastic properties, with the highest values of planar frequency

Table 2
Grain size distribution parameters of hot-pressed $NaNbO_3$ ceramics. Values shown for samples marked with asterisk correspond to the measurable grain size distribution of the bimodal type distribution observed in these samples.

| Grain distribution | | | | | |
|---|---|---|---|---|---|
| Precursor | Hot-pressing temperature | Mean grain size $G$ (nm) | Standard deviation $\sigma_G$ (nm) | Number of measured grains $N_G$ | Piezoelectric coefficient $d_{33}$ ($pC\,N^{-1}$) |
| C-NN | 1000 °C | 220 | 120 | 414 | 40 |
| NOH-NN | 1000 °C | 170 | 90 | 916 | 6 |
| O-NN | 1000 °C* | 110 | 50 | 888 | 6 |
| | 1100 °C | 240 | 120 | 879 | 24 |
| DOH-NN | 1000 °C* | 160 | 80 | 409 | 38 |
| | 1100 °C | 390 | 230 | 666 | 32 |

Table 3
Dielectric, elastic, piezoelectric and electromechanical coupling factors corresponding to the radial resonance mode for hot-pressed $NaNbO_3$ ceramics.

| $NaNbO_3$ ceramic type | C-NN 1000 °C | O-NN 1100 °C | DOH-NN 1000 °C | DOH-NN 1100 °C |
|---|---|---|---|---|
| Planar coupling factor $k_p$ (%) | 14 | 8 | 12 | 12 |
| Planar frequency number $N_p$ (kHz mm) | 3571 | 3535 | 3252 | 3778 |
| Elastic stiffness $c_{11}^{P}$ ($10^{-10}\,N\,m^{-2}$) | 12.8 + 0.06i | 13.6 + 0.02i | 10.9 + 0.02i | 15.7 + 0.02i |
| Elastic compliance $s_{11}^{E}$ ($10^{-12}\,m^2\,N^{-1}$) | 8.5–0.04i | 7.8–0.01i | 9.7–0.03i | 6.7–0.008i |
| Piezoelectric coefficient $d_{31}$ ($10^{-12}\,C\,N^{-1}$) | −8.7 + 0.09i | −7.2 + 0. 03i | −7.8 + 0.06i | −7.2 + 0.03i |
| Relative permittivity $\varepsilon_{33}^{T}$ | 144 + 1.77i | 154 + 1.44i | 133 + 1.64i | 158 + 1.79i |

number ($N_p = 3778$ kHz mm) and the elastic stiffness ($c_{11}^{P} = 15.7\,N\,m^{-2}$).

## 4. Discussion

Fig. 1 shows that pressure-less sintering of mechanochemical activated precursors produces single-phase ceramics in a single thermal process, in which synthesis, sintering and grain growth take place. It is due to the reduction by mechanical activation of the thermal barrier necessary to activate the process. However, the density obtained at the same sintering temperature is different for each precursor. For the C-NN sintered ceramic is lower than the green pellet one because of the well-known effect of the use of carbonates that produce $CO_2$, which is very volatile, during the thermal treatment.[43] It hinders the sintering and the closure of porosity. Moreover, the C-NN precursor is less reactive[36,43] than the other ones, as a higher temperature and a larger time is needed to isolate the phase. The changes in the state of $Nb_2O_5$ (particle size and microstrains) during milling are negatively affected by the simultaneously activation with $NaCO_3$,[30] reducing the total reactivity of the mixture.

The ceramics obtained by the other precursors show lower porosity (4.5% for O-NN and 3.0% for DOH-NN) whilst using lower processing temperatures, than those found in the literature for $NaNbO_3$ ceramics sintered from solid-state reaction precursors (4%, at 1240 °C, in two steps,[44] 5% at 1550 °C[45]) or chemical routes (5%, at 1250 °C).[12]

As it was said, the problem with pressure-less sintering is that the ceramics reach a high density but they are easily cracked. Although the surface reactivity of the mechanically activated powder particles improves the surface mass transport needed for the sintering process and closure of the interparticle porosity, the resulting bonding between particles seems to be weak, most probably by accumulation in grain boundaries of crystal defects migrated to the surface. The presence of agglomerates may also yield to non homogenous microstructures (in pore and grain size distribution) that could contribute to the cracking. This is critical for piezoelectric applications, in which a poor mechanical resistance affects the long life of the material under vibration or repeated actuation. The use of the hot-pressing solves that problem.

Fig. 3 shows that a single-phase ceramic can be also obtained in a one-step thermal treatment by hot-pressing. Exceptions are C-NN at 900 °C or O-NN at 1000 °C ceramics. It seems that it is due to the low hot-pressing temperature, not enough for this not so high reactive precursor to synthesize a single phase. The secondary phase can be indexed as $Na_2Nb_4O_{11}$ (JCPDF ICPD file no. 72-1694), also observed during the thermal treatment of powders after the mechanical activation of the O-NN precursors.[36] The phase $Na_2Nb_4O_{11}$ also appears as an intermediate phase when traditional solid-state reaction is used. It indicates that O-NN precursors have a lower reactivity than the others, which also affects, as Fig. 4 shows, to the porosity content of the ceramics. The main contribution to the porosity comes from the inter-agglomerates space. It increases the porosity (6%), as Table 1 shows. An increase of the hot-pressing temperature from 1000 to 1100 °C makes the secondary phase to disappear (Fig. 3) and a decrease in the porosity (from 6 to 3.8%). Consequently, there is also an important reduction in the pore area (from 4.2 to 0.9 $\mu m^2$).

DOH-NN precursors give the lowest values of porosity of the hot-pressed ceramics (only 0.40% for 1000 °C). A further increase of the hot-pressing temperature to 1100 °C produces a slight increase in the porosity (to 2.10%, Table 1), due to the

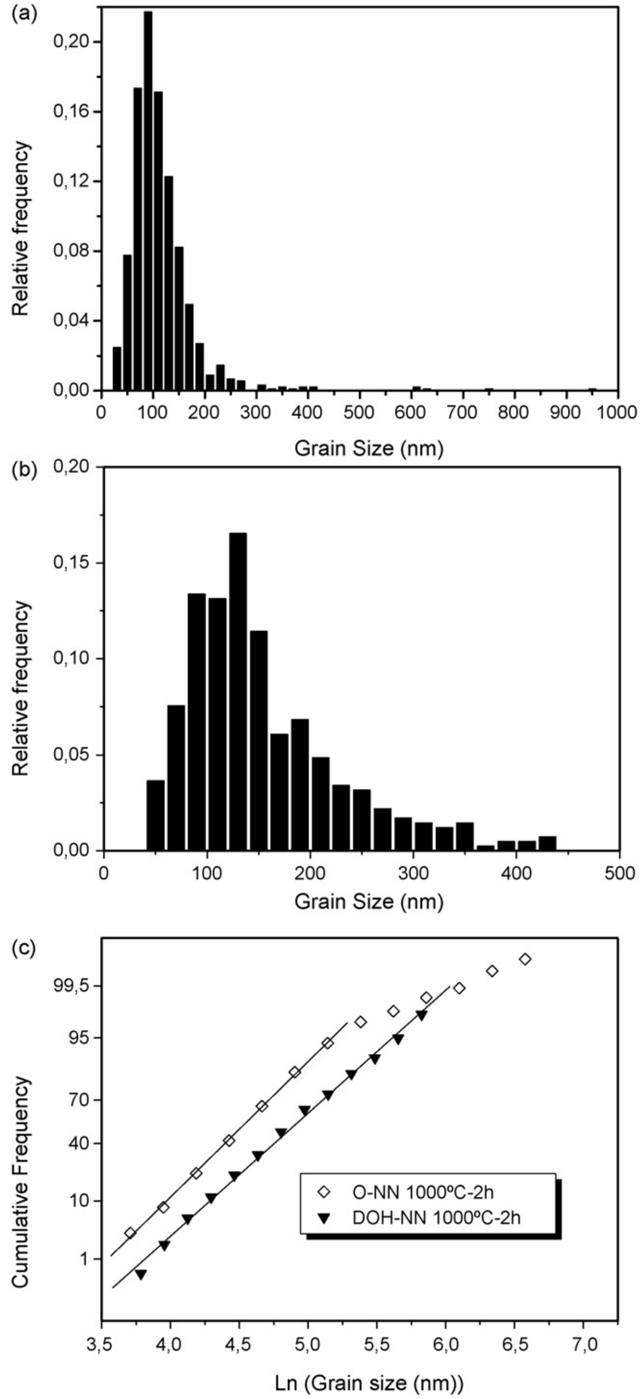

Fig. 7. Asymmetric and bimodal grain size distributions and corresponding probability plots, from the corresponding distributions of logarithm of the grain size, for the hot-pressed ceramics that present very fine structured areas: (a) O-NN 1000 °C and (b) DOH-NN 1000 °C. Lines of the probability plots (c) correspond to the fitting of the measurable grain size distributions, whose parameters are presented in Table 2.

decrease in the ratio between sintering and grain growth rate, which is characteristic of a degraded sintering stage.

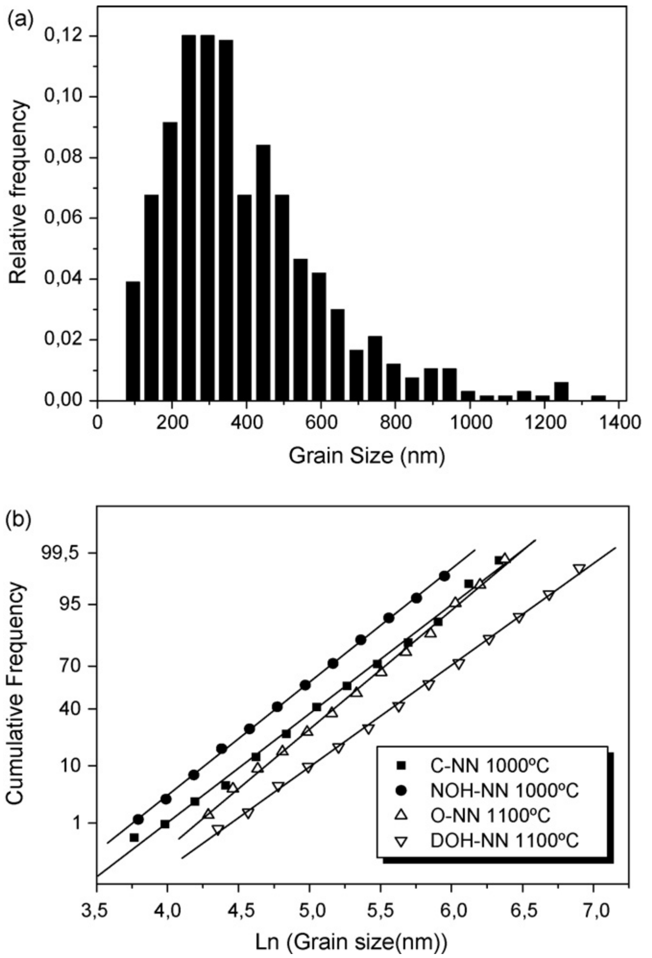

Fig. 8. (a) Grain size distributions and (b) corresponding probability plots, from the corresponding distributions of logarithm of the grain size for hot-pressed $NaNbO_3$ ceramics: C-NN 1000 °C; NOH-NN 1000 °C; O-NN 1100 °C; DOH-NN 1100 °C. The grain size distribution of the last ceramic, a single lognormal distribution, is presented for comparison with distributions shown in Fig. 7.

The residual porosity is reduced with respect to the reported for other alkaline-niobate ceramics prepared by hot-pressing of $Li_{1-x}Na_xNbO_3$[6] (>10% at 1100 °C), in which the presence of light Li atoms promotes the mass transport. The residual porosity is also lower than that achieved using other pressure-assisted processing methods, as spark plasma sintering by Wada et al.[8] (6% at 1200 °C for $NaNbO_3$ ceramics) or Zhang et al.[9] (8% at 920 °C for $Na_xK_{1-x}NbO_3$ with $x = 0.20$, where the presence of K also improves the sinterability). In both cases precursors obtained by traditional solid-state reaction were used. An important advantage of the use in this work of lower processing temperatures is that helps preventing the evaporation of the large amounts of alkaline elements.

The grain size distributions are very inhomogeneous for the ceramics hot-pressed at 1000 °C from NOH, and much more from O-NN and DOH-NN precursors, as Fig. 6 shows. This is usually related with incomplete sintering stages of various types. For O-NN precursor it could be due to inhomogeneity by the presence of the secondary phase observed in Fig. 3, which gives place to larger grains observed in Fig. 6. An increase of the temperature solves the problem, and the ceramic hot-pressed at 1100 °C from O-NN precursor has a more homogeneous microstructure as the comparison of the slopes of the probability plots of the grain size distributions shows (Figs. 7 and 8). The mean grain size and standard deviation of the corresponding distribution for 1100 °C O-NN ceramic is still relatively small (240 nm and 120 nm), even when compared with the grain size of the ceramics from C-NN (220 and 120 nm) hot-pressed at 1000 °C. These results confirm the lower reactivity of the O-NN precursor with respect to the other ones studied.

The incomplete sintering at 1000 °C from DOH-NN ceramic seems to have different causes than for O-NN ones, as no secondary phases were found for this ceramic. It has been reported[46] that growth in $NaNbO_3$ during calcination from homogeneous amorphous polymeric precursors occurs in two steps. Up to temperatures ~300 °C higher than the synthesis one, a process of neck formation and growth controlled by surface diffusion occurs, filling the necks among particles. In a second stage, the densification of agglomerates takes place, and the particle growth increases substantially in comparison to the crystallite growth. A further increase of temperature increases the particle size by a process of grain boundary migration. Similarly, during hot-pressing, the low temperature processes and the densification of agglomerates are favoured, improving the density of the ceramics. The presence of the clusters in the DOH-NN ceramic hot-pressed at 1000 °C, from which larger grains are grown, seems to indicate that grain boundary migration is not complete. It favours the low porosity achieved with respect to the other precursors, but at temperatures as low as 1000 °C the grain distribution is still bimodal. A further increase of temperature to 1100 °C increases the grain boundary migration and the homogeneity of the grain size.

Table 2 also shows the $d_{33}$ piezoelectric coefficient of the hot-pressed ceramics. The lower values ($d_{33} = 6\,\mathrm{pC\,N^{-1}}$) obtained for the ceramics processed at 1000 °C from O-NN and NOH-NN precursors are a consequence of the low polarizability of those ceramics, already discussed. For ceramics from C-NN and DOH-NN precursors it was possible to pole the ceramics up to saturation at 180 °C with fields of 60 kV/cm, which explains the slightly higher piezoelectric coefficients obtained.

The hot-pressed from C-NN precursor ceramic presents the highest piezoelectric activity, with values of $k_p = 14\%$, $d_{31} = -8.7\,\mathrm{pC\,N^{-1}}$ and $d_{33} = 40\,\mathrm{pC\,N^{-1}}$. These results slightly improve the obtained by Reznitchenko et al.[44] ($k_p = 10\%$) in ceramics processed by classical methods. Values up to $k_p = 19\%$ have been obtained by Wada et al.[8] in spark plasma sintered ceramics (with grain size range of 3–5 μm). Although all these values are of the same order, the comparison with results in this work is not straightforward, since the method here used is not the IEEE Standard, currently used, but a much more accurate one in the calculation of moderate electromechanical coupling coefficients.

However, it is noticeable that our values are obtained for highly dense submicron-structured ceramics, in agreement with previous works where samples with grain size in the order of 200–300 nm improves the piezoresponse measured by PFM with respect to coarser grain ceramics.[35] The most remarkable result is the ensemble of piezoelectric and elastic properties ($k_p = 12\%$ and $d_{31} = -7.8\,\mathrm{pC\,N^{-1}}$ and $d_{33} = 38\,\mathrm{pC\,N^{-1}}$, on the one hand, and $N_p = 3252\,\mathrm{kHz\,mm}$ and $s^E_{11} = (9.7 - 0.03i)\,10^{-12}\,\mathrm{m^2\,N^{-1}}$, on the other hand) that was measured for DOH-NN ceramic hot-pressed at 1000 °C with a microstructure characterized by 0.40% residual porosity and a bimodal lognormal distribution of grain size, with average value of 160 nm for the well defined population of higher grain size.

The microstructures obtained in this work also results in good mechanical properties, although comparison with other author results in this point cannot be made. Slight improvement in the elastic properties by means of the homogenisation of the microstructure in these submicron-structured ceramics is also revealed in the study. The ceramic hot-pressed at 1100 °C from DOH-NN precursor has the highest frequency planar number ($N_p = 3778\,\mathrm{kHz\,mm}$) and the lower complex elastic compliance (($s^E_{11}(6.7 - 0.008i)\,10^{-12}\,\mathrm{m^2\,N^{-1}}$) of all the ceramics. The higher homogeneity of the corresponding microstructure is evidenced by the comparison of the grain size distribution of this ceramic in Fig. 8 with those of the complex microstructures in Fig. 7.

## 5. Conclusions

Ceramics of composition $NaNbO_3$ have been prepared from precursors obtained by four different routes of mechanical activation. Single-phase ceramics are obtained in one-step thermal treatment.

The porosity of the pressure-less sintered is lower than the obtained from solid-state reaction while allows using lower temperatures. However, they have poor mechanical stability that prevents their practical use.

Hot-pressing allows obtaining highly dense (with contents of porosity down to 0.4%) and mechanically stable submicron-structured ceramics. Homogenous microstructures with single lognormal distributions and submicron average grain size can be obtained, together with residual porosities of 1.5 and 2.10%, respectively. This submicron-structured ceramics is as a consequence of the low particle size of the powder precursors and the low processing temperatures needed when mechanically activated precursors are used. When hot-pressing conditions are not optimized, intermediate stages of sintering are observed and bimodal lognormal distributions of grain size are measured.

A noticeable ensemble of piezoelectric and elastic properties was measured for DOH-NN ceramic hot-pressed at 1000 °C. The observed changes of the functional properties of the ceramics were not high and were related to microstructural characteristics. The highest piezoelectric activity was characterized by values of $k_p = 14\%$ and $d_{31} = -8.7\,\mathrm{pC\,N^{-1}}$ and $d_{33} = 40\,\mathrm{pC\,N^{-1}}$. The best elastic properties of the ceramics were characterized by values of $N_p = 3778\,\mathrm{kHz\,mm}$ and $s^E_{11}(6.7 - 0.008i)\,10^{-12}\,\mathrm{m^2\,N^{-1}}$ and related with the homogeneity of the submicron-structured microstructure that shows a single lognormal distribution.

## Acknowledgements

This work was funded by EC project "LEAF" G5RD-CT2001-00431 and MAT2001-4818E (MCyT Spain). Drs. A.

Moure and T. Hungría are indebted to the CSIC (MICINN) of Spain for the "Junta de Ampliación de Estudios" contracts (Refs JAEDOC087 and JAEDOC082, respectively). Thanks are also given to Ms. M. Antón for the powder samples preparation.

## References

1. European Union Directive 2002/95/EC on the Restriction Of the use of certain Hazardous Substances in electrical and electronic equipment (RoHS directive), available at http://www.crouzet-usa.com/RoHS.pdf.).
2. Cross, E., Materials science—lead-free at last. *Nature*, 2004, **432**, 24–25.
3. Saito, Y., Takao, H., Tani, T., Nonoyama, T., Takatori, K., Homma, T., Nagaya, T. and Nakamura, M., Lead-free piezoceramics. *Nature*, 2004, **432**, 84–87.
4. Shrout, T. R. and Zhang, S. J., Lead-free piezoelectric ceramics: Alternatives for PZT? *J. Electroceram.*, 2007, **19**, 111–124.
5. Nitta, T., Properties of sodium-lithium niobate solid solution ceramics with small lithium concentrations. *J. Am. Ceram. Soc.*, 1968, **51**, 626–629.
6. Henson, R. M., Zeyfang, R. R. and Kiehl, K. V., Dielectric and electromechanical properties of (Li, Na)NbO$_3$ ceramics. *J. Am. Ceram. Soc.*, 1977, **60**, 15–17.
7. Hardiman, B., Henson, R. M., Reeves, C. P. and Zeyfang, R. R., Hot-pressing of sodium lithium-niobate ceramics with perovskite-like structures. *Ferroelectrics*, 1976, **12**, 157–159.
8. Wada, T., Tsuji, K., Saito, T. and Matsuo, Y., Ferroelectric NaNbO$_3$ ceramics fabricated by spark plasma sintering. *Jpn. J. Appl. Phys.*, 2003, **42**, 6110–6114.
9. Zhang, B. P., Li, J. F., Wang, K. and Zhang, H., Compositional dependence of piezoelectric properties in Na$_x$K$_{1-x}$NbO$_3$ lead-free ceramics prepared by spark plasma sintering. *J. Am. Ceram. Soc.*, 2006, **89**, 1605–1609.
10. Cross, L. E. and Nicholson, B., The optical and electrical properties of single crystals of sodium niobate. *J. Phil. Magn. Ser.*, 1955, **46**, 453–466.
11. Shirane, G., Newnham, B. and Pepinsky, R., Dielectric properties and phase transitions of NaNbO$_3$ and (Na,K)NbO$_3$. *Phys. Rev.*, 1954, **96**, 581–588.
12. Lanfredi, S., Dessemond, L. and Rodrigues, A. C., Dense ceramics of NaNbO$_3$ produced from powders prepared by a new chemical route. *J. Eur. Ceram. Soc.*, 2000, **20**, 983–990.
13. Nibou, L., Manier, M. and Mercurio, J. P., LiNbO$_3$-based piezoelectric ceramics prepared from sol-gel derived powders. *Ann. Chim. Sci. Mater.*, 1998, **23**, 135–138.
14. Goh, G. K. L., Lange, F. F., Haile, S. M. and Levi, C. G., Hydrothermal synthesis of KNbO$_3$ and NaNbO$_3$ powders. *J. Mater. Res.*, 2003, **18**, 338–345.
15. Paula, A. J., Zaghete, M. A., Longo, E. and Varela, J. A., Microwave-assisted hydrothermal synthesis of structurally and morphologically controlled sodium niobates by using niobic acid as a precursor. *Eur. J. Inorg. Chem.*, 2008, **8**, 1300–1308.
16. Camargo, E. R., Popa, M. and Kakihana, M., Sodium niobate (NaNbO$_3$) powders synthesized by a wet-chemical method using a water-soluble malic acid complex. *Chem. Mater.*, 2002, **14**, 2365–2368.
17. Pithan, C., Shiratori, Y., Dornseiffer, J., Haegel, F. H., Magrez, A. and Waser, R., Microemulsion mediated synthesis of nanocrystalline (K$_x$,Na$_{1-x}$)NbO$_3$ powders. *J. Cryst. Growth*, 2005, **280**, 191–200.
18. Samuel, V., Gaikwad, A. B. and Ravi, V., A coprecipitation technique to prepare NaNbO$_3$ and NaTaO$_3$. *Bull. Mater. Sci.*, 2006, **29**, 123–125.
19. Xue, J. M., Wan, D. M., Lee, S. E. and Wang, J., Inducing crystallization in an amorphous lead zirconate titanate precursor by mechanical activation. *J. Am. Ceram. Soc.*, 1999, **82**, 1641–1643.
20. Wang, J., Xue, J. M., Wan, D. M. and Gan, B. K., Mechanically activating nucleation and growth of complex perovskites. *J. Solid State Chem.*, 2000, **154**, 321–328.
21. Alguero, M., Ricote, J., Hungría, T. and Castro, A., High-sensitivity piezoelectric, low-tolerance-factor perovskites by mechanosynthesis. *Chem. Mater.*, 2007, **19**, 4982–4990.
22. Lisoni, J. G., Millán, P., Vila, E., Martín de Vidales, J. L., Hoffman, T. and Castro, A., Synthesis of ferroelectric Bi$_4$Ti$_3$O$_{12}$ by alternative routes: wet no-coprecipitation chemistry and mechanochemical activation. *Chem. Mater.*, 2001, **13**, 2084–2091.
23. Ng, S. H., Xue, J. M. and Wang, J., Bismuth titanate from mechanical activation of a chemically coprecipitated precursor. *J. Am. Ceram. Soc.*, 2002, **85**, 2660–2665.
24. Kong, L. B., Zhang, T. S., Ma, J. and Boey, F., Progress in synthesis of ferroelectric ceramic materials via high-energy mechanochemical technique. *Prog. Mater. Sci.*, 2008, **53**, 207–322.
25. Castro, A., Millán, P., Pardo, L. and Jiménez, B., Synthesis and sintering improvement of Aurivillius type structure ferroelectric ceramics by mechanochemical activation. *J. Mater. Chem.*, 1999, **9**, 1313–1317.
26. Lee, S. E., Xue, J. M., Wan, D. M. and Wang, J., Effects of mechanical activation on the sintering and dielectric properties of oxide derived PZT. *Acta Mater.*, 1999, **47**, 2633–2639.
27. Pardo, L., Castro, A., Millán, P., Alemany, C., Jiménez, R. and Jiménez, B., (Bi$_3$TiNbO$_9$)$_x$(SrBi$_2$Nb$_2$O$_9$)$_{1-x}$ Aurivillius type structure piezoelectric ceramics obtained from mechanochemically activated oxides. *Acta Mater.*, 2001, **48**, 2421–2428.
28. Moure, A., Castro, A. and Pardo, L., Improvement by-recrystallisation of Aurivillius-type structure piezoceramics from mechanically activated precursors. *Acta Mater.*, 2004, **52**, 945–957.
29. Rojac, T., Masson, O., Guinebretiere, R., Kosec, M., Malic, B. and Holc, J., A study of the mechanochemical synthesis of NaNbO$_3$. *J. Eur. Ceram. Soc.*, 2007, **27**, 2265–2271.
30. Rojac, T., Kosec, M., Malic, B. and Holc, J., The mechanochemical synthesis of NaNbO$_3$ using different ball-impact energies. *J. Am. Ceram. Soc.*, 2008, **91**, 1559–1565.
31. Okazaki, K. and Nagata, K., Effects of grain size and porosity on electrical and optical properties of PLZT ceramics. *J. Am. Ceram. Soc.*, 1973, **56**, 82–86.
32. Yamamoto, T., Optimum preparation methods for piezoelectric ceramics and their evaluation. *Am. Ceram. Soc. Bull.*, 1992, **71**, 978–985.
33. Randall, C. A., Kim, N., Kucera, J. P., Cao, W. and Shrout, T. R., Intrinsic and extrinsic size effects in fine-grained morphotropic-phase-boundary lead zirconate titanate ceramics. *J. Am. Ceram. Soc.*, 1998, **81**, 677–688.
34. Shiratori, Y., Magrez, A., Dornseiffer, J., Haegel, F. H., Pithan, C. and Waser, R., Polymorphism in micro-, submicro-, and nanocrystalline NaNbO$_3$. *J. Phys. Chem. B*, 2005, **109**, 20122–20130.
35. Shiratori, Y., Magrez, A., Kasezawa, K., Kato, M., Röhrig, S., Peter, F., Pithan, C. and Waser, R., Noncentrosymmetric phase of submicron NaNbO$_3$ crystallites. *J. Electroceram.*, 2007, **19**, 273–280.
36. Hungría, T., Castro, A., Moure, A. and Pardo, L., Effect of mechanochemical activation on the synthesis of NaNbO$_3$ and processing of environmentally friendly piezoceramics. *J. Alloys Compd.*, 2005, **395**, 166–173.
37. Ricote, J. and Pardo, L., Microstructure-properties relationships in samarium modified lead titanate piezoceramics. 1. Quantitative study of the microstructure. *Acta Mater.*, 1996, **44**, 1155–1167.
38. Kurtz, S. K. and Carpay, F. M. A., Microstructure and normal grain-growth in metals and ceramics 2. Experiment. *J. Appl. Phys.*, 1980, **51**, 5745–5754.
39. Alemany, C., Gónzalez, A. M., Pardo, L., Jiménez, B., Carmona, F. and Mendiola, J., Automatic-determination of complex constants of piezoelectric lossy materials in the radial mode. *J. Phys. D: Appl. Phys.*, 1995, **28**, 945–956.
40. Rossignol, F., Goursat, P. and Besson, J. L., Microstructure and mechanical behaviour of self-reinforced Si$_3$N$_4$ and Si$_3$N$_4$-SiC whisker composites. *J. Eur. Ceram. Soc.*, 1994, **13**, 299–312.
41. Moure, A., Pardo, L., Alemany, C., Millán, P. and Castro, A., Piezoelectric ceramics based on Bi$_3$TiNbO$_9$ from mechanochemically activated precursors. *J. Eur. Ceram. Soc.*, 2001, **21**, 1399–1402.
42. Antou, G., Montavon, G., Hlawka, F., Cornet, A. and Coddet, C., Microstructures of partially stabilized zirconia manufactured via hybrid plasma spray process. *Ceram. Int.*, 2005, **31**, 611–619.
43. Castro, A., Jiménez, B., Hungría, T., Moure, A. and Pardo, L., Sodium niobate ceramics prepared by mechanical activation assisted methods. *J. Eur. Ceram. Soc.*, 2004, **24**, 941–945.

44. Reznitchenko, L. A., Turik, A. V., Kuznetsova, E. M. and Sakhnenko, V. P., Piezoelectricity in $NaNbO_3$ ceramics. *J. Phys. Condens. Matter*, 2001, **13**, 3875–3881.
45. Raevski, I. P. and Prosandeev, S. A., A new, lead free, family of perovskites with a diffuse phase transition: $NaNbO_3$-based solid solutions. *J. Phys. Chem. Solids*, 2002, **63**, 1939–1950.
46. Leite, E. R., Nobre, M. A. L., Cerqueira, M., Longo, E. and Varela, J. A., Particle growth during calcination of polycation oxides synthesized by the polymeric precursors method. *J. Am. Ceram. Soc.*, 1997, **80**, 2649–2657.